Seismic and Episodic Slip Characteristics of Frictional-Viscous Subduction Megathrust Shear Zones

Whitney M. Behr[1], Taras V. Gerya[2], Claudio Cannizzaro[3], and Robert Blass[3]

[1]Department of Earth Sciences, ETH Zürich
[2]Swiss Federal Institute of Technology (ETH-Zurich)
[3]ETH Zurich

November 24, 2022

Abstract

The deep roots of subduction megathrusts exhibit aseismic slow slip events, commonly accompanied by tectonic tremor. Observations from exhumed rocks suggest this region of the subduction interface is a shear zone with frictional lenses embedded in a viscous matrix. Here we use numerical models to explore the transient slip characteristics of finite-width frictional-viscous megathrust shear zones. Our model utilizes an invariant, continuum-based, regularized form of rate- and state-dependent friction (RSF) and simulates earthquakes along spontaneously evolving faults embedded in a 2D heterogeneous continuum. The setup includes two elastic plates bounding a viscoelastoplastic shear zone (subduction interface melange) with inclusions (clasts) of varying distributions and viscosity contrasts with respect to the surrounding weaker matrix. The entire shear zone exhibits the same velocity-weakening RSF parameters, but the lower viscosity matrix has the capacity to switch between RSF and viscous creep as a function of local stress state. Results show that for a range of matrix viscosities near the frictional-viscous transition, viscous damping and stress heterogeneity in these shear zones both 1) sets the 'speed limit' for earthquake ruptures that nucleate in clasts such that they propagate at slow velocities; and 2) permits the transmission of slow slip from clast to clast, allowing slow ruptures to propagate substantial distances over the model domain. For reasonable input parameters, modeled events have moment-duration statistics, stress drops, and rupture propagation rates that match natural slow slip events. These results provide new insights into how geologic observations from ancient analogs of the slow slip source may scale up to match geophysical constraints on modern slow slip phenomena.

Seismic and Episodic Slip Characteristics of Frictional-Viscous Subduction Megathrust Shear Zones

Behr, Whitney Maria[1], Gerya, Taras[1], Cannizzaro, C.[2], Blass, R.[2]

[1]Department of Earth Sciences, Swiss Federal Institute of Technology (ETH), Zurich, Switzlerand
[2]Department of Mathematics, Swiss Federal Institute of Technology (ETH), Zurich, Switzlerand

Key Points:

- Models of frictional-viscous megathrust melanges predict a wide range of transient slip styles.
- Viscous damping and stress heterogeneity in a melange matrix sets the speed limit for slip.
- Ruptures in melange belts can propagate long distances and link up heterogeneities at slow speeds

Corresponding author: Whitney Behr, `wbehr@ethz.ch`

Abstract

The deep roots of subduction megathrusts exhibit aseismic slow slip events, commonly accompanied by tectonic tremor. Observations from exhumed rocks suggest this region of the subduction interface is a shear zone with frictional lenses embedded in a viscous matrix. Here we use numerical models to explore the transient slip characteristics of finite-width frictional-viscous megathrust shear zones. Our model utilizes an invariant, continuum-based, regularized form of rate- and state-dependent friction (RSF) and simulates earthquakes along spontaneously evolving faults embedded in a 2D heterogeneous continuum. The setup includes two elastic plates bounding a viscoelastoplastic shear zone (subduction interface melange) with inclusions (clasts) of varying distributions and viscosity contrasts with respect to the surrounding weaker matrix. The entire shear zone exhibits the same velocity-weakening RSF parameters, but the lower viscosity matrix has the capacity to switch between RSF and viscous creep as a function of local stress state. Results show that for a range of matrix viscosities near the frictional-viscous transition, viscous damping and stress heterogeneity in these shear zones both 1) sets the 'speed limit' for earthquake ruptures that nucleate in clasts such that they propagate at slow velocities; and 2) permits the transmission of slow slip from clast to clast, allowing slow ruptures to propagate substantial distances over the model domain. For reasonable input parameters, modeled events have moment-duration statistics, stress drops, and rupture propagation rates that match natural slow slip events. These results provide new insights into how geologic observations from ancient analogs of the slow slip source may scale up to match geophysical constraints on modern slow slip phenomena.

Plain Language Summary

Subduction megathrusts represent the largest and most hazardous seismogenic faults on Earth and exhibit a wide range of earthquake slip patterns. An especially perplexing form of slip on subduction megathrusts are 'slow earthquakes', which are slip events that release similar amounts of energy as regular earthquakes, but do so over months to years, rather than seconds. These events most commonly occur at deeper levels of the subduction megathrust where rocks are thought to transition from brittle and strong— with deformation dominated by fracture and cracking— to smoother, continuous, and weak— with deformation dominated by flow. In this work, we use numerical models to explore the seismic slip characteristics of megathrust faults that are mixtures of weak and strong materials. We simulate a wide megathrust fault zone with embedded weak and strong sections, and we systematically vary the strength contrasts between, and relative proportions of, weak to strong material. Our results suggest that three regimes of slip behaviors can be defined as a function of these strength contrasts and proportions of weak-to-strong materials: an aseismic regime with no earthquake slip, a slow-slip dominated regime, and a regular earthquake-dominated regime. These results help to reconcile some of the features that geologists find in rock outcrops brought to the surface from deep subduction environments, with the modern-day geophysical record of subduction zone earthquakes and surface deformation patterns.

1 Introduction

Deep episodic slow slip events (SSEs), commonly accompanied by non-volcanic tremor and low-frequency earthquakes, are increasingly recognized as essential processes of strain release in subduction zones (Beroza & Ide, 2011; Lay et al., 2012; Z. Peng & Gomberg, 2010; Rousset et al., 2019; Shelly et al., 2007) and continental plate boundary faults (Chen et al., 2018; Shelly, 2017; Thomas et al., 2009; Wech et al., 2012). In subduction environments, SSEs typically occur at and around the mantle wedge corner, down-dip of the seismogenic megathrust in what is thought to be an environment rich in metamorphic reactions and associated fluids, and high fluid pressures (Audet & Bürgmann, 2014; Audet & Kim, 2016;

Behr & Bürgmann, 2021; Condit et al., 2020; Peacock, 2009). SSEs can reach similar magnitudes to 'regular' megathrust earthquakes, but they exhibit much slower slip rates (∼1-2 mm/day), smaller displacements (mm to a few cm), longer durations (days to years), more frequent recurrence (months to years), and lower stress drops (∼1-100 kPa) (Bletery & Nocquet, 2020; Michel et al., 2019; Obara & Sekine, 2009; Schmidt & Gao, 2010; Wallace & Eberhart-Phillips, 2013; Wech & Bartlow, 2014). Understanding the physical mechanisms controlling SSEs, their similarities and differences compared to high-frequency earthquakes, and their role in priming or directly triggering megathrust slip is a fundamental challenge in geodynamics.

Since the original detection of slow slip events, a wide range of numerical simulations have been used to explore potential source mechanisms. Several aspects of SSEs can be reproduced using numerical models of frictional sliding on a discrete, planar fault within a rate-and-state-friction framework (J. H. Dieterich, 1979; Marone, 1998; Rubin, 2008; Ruina, 1983). Liu & Rice (2005), for example, demonstrated that aseismic slip transients arise where faults transition with depth/temperature from velocity-weakening to velocity-strengthening frictional properties. Skarbek et al. (2012) similarly showed that mixtures of velocity-weakening and -strengthening materials on a fault could control the sliding behavior, with slow slip favored by velocity-weakening to -strengthening material ratios of 40-70%. Several models have also coupled rate-and-state friction and dilatancy with elasticity and pore-fluid-pressure diffusion, suggesting that dilatant strengthening competes with fault thermal or poro-plasto-elastic pressurization to modulate fault slip rates over a range comparable to natural faults (Liu & Rubin, 2010; Petrini et al., 2020; Segall & Bradley, 2012; Segall et al., 2010; Suzuki & Yamashita, 2009). Other model types that invoke a velocity-dependent friction law, e.g. faults that transition from rate-weakening at low slip rates to neutral or rate-strengthening at higher slip rates, expand the range of parameter-space over which slow slip-type behavior can be produced (e.g. Beeler, 2009; Hawthorne & Rubin, 2013; Im et al., 2020; Shibazaki, 2003).

Although planar megathrust fault models with varying frictional and/or poroelastic properties are successful at reproducing a spectrum of fault slip behaviors, the model framework of a discrete fault surface or thin gouge layer is challenging to reconcile with geophysical imaging of modern SSE environments, and with geologic observations of rocks exhumed from SSE source depths. Seismic reflection, tomography, and receiver function images, for example, show that the deep SSE source region coincides with a seismic low velocity and low V_p-V_s ratio zone that is up to several kilometers in thickness, interpreted to represent a 'subduction channel' or wide subduction shear zone composed of underplated, heterogeneous, subduction melange material (Audet & Schaeffer, 2018; Calvert, 1996; Calvert et al., 2020; Delph et al., 2018; Hansen et al., 2012; Li et al., 2015; Nedimović et al., 2003). Geological observations from exhumed rocks support this notion of a finite-width subduction shear zone on the deep interface (e.g. Behr & Platt, 2013; Cloos & Shreve, 1988; Festa et al., 2010; Grigull et al., 2012; Xia & Platt, 2017), and furthermore suggest that deformation within it proceeds by coupled frictional sliding and viscous creep (Angiboust et al., 2011a; Fagereng & Den Hartog, 2017; Fagereng & Sibson, 2010; Hayman & Lavier, 2014; Ujiie et al., 2018). Observations from the outcrop scale, for example, commonly include block-in-matrix melanges in which rigid, cm- to m-scale lenses concentrate brittle slip along geometrically complex, interconnected fault networks hosted within a ductile matrix (Cowan, 1985; Fagereng, 2011; Fagereng et al., 2014; Fisher & Byrne, 1987; Kotowski & Behr, 2019; Phillips et al., 2020). These outcrop-scale features are mimicked at the multi-kilometric scale with map patterns of exhumed subduction complexes containing underplated mafic or ultramafic lineaments mantled by high-strain, viscous melange belts (Agard et al., 2018; Tewksbury-Christle et al., 2021). These finite-width, heterogeneous shear zones are so commonly preserved in the rock record that understanding their potential for seismic or transient slip on the deep interface seems essential to understanding the processes occurring within the SSE zone (cf. Beall et al., 2019; Behr & Bürgmann, 2021; Fagereng & Sibson, 2010; Hayman & Lavier, 2014; Lavier et al., 2021; Skarbek et al., 2012).

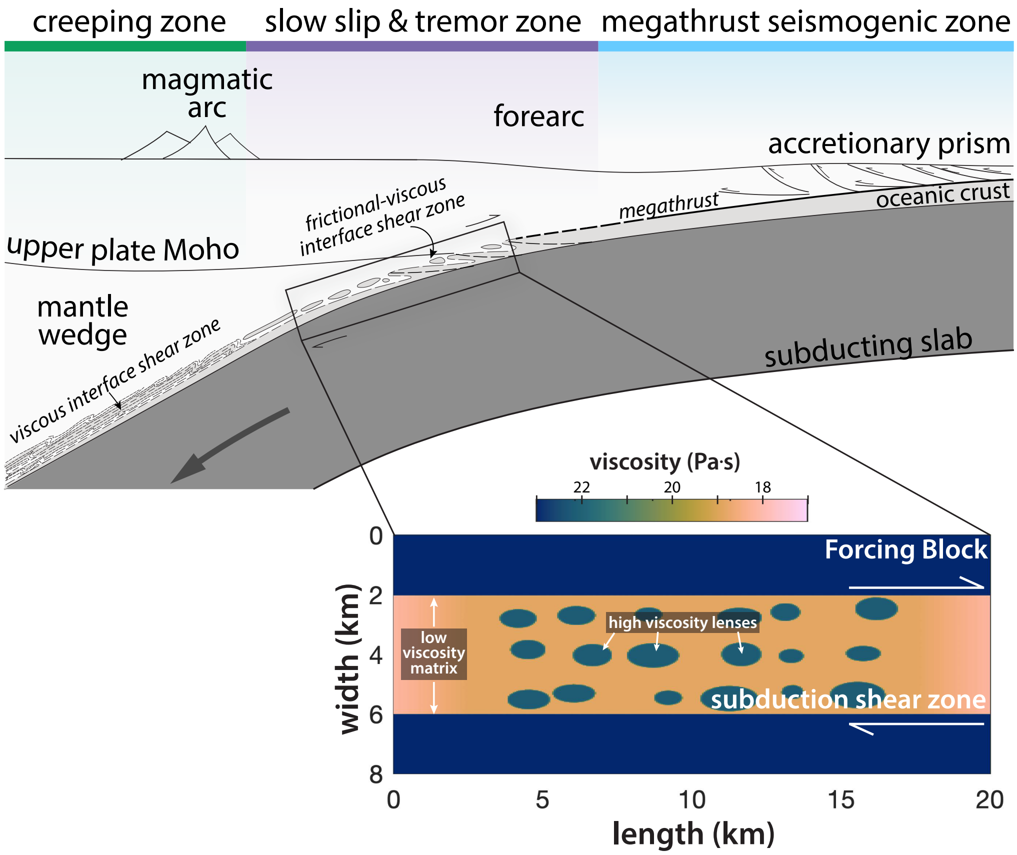

Figure 1. A) Schematic sketch of the subduction interface and associated transitions in structural style and seismic behavior with depth. The subduction interface has been suggested to transition downdip near the depth of slow slip and tremor from a discrete frictional megathrust fault to a more distributed frictional-viscous shear zone, which is the basis for the model setup shown in b). B) Model setup investigated here with high viscosity inclusions (clasts) embedded in a lower viscosity matrix and sheared at a constant boundary velocity.

Here we use numerical models, inspired by geophysical and geological observations of the SSE source region, to investigate the transient slip characteristics of distributed frictional-viscous shear zones. We build upon previous rate-and-state-friction-based models, but combine this model framework with visco-elasto-plastic deformation of a heterogeneous continuum to explore the interplay between viscous shear zone loading, brittle-plastic yielding, and rate-dependent frictional sliding on spontaneously generated slip surfaces embedded within a finite-width shear zone representative of subduction "mega-melange". We examine qualitative and quantitative similarities between modeled events and natural fast and slow-slip and discuss implications for slow slip source mechanisms. Our results can potentially reconcile geophysical constraints on slow slip phenomena with the exhumed geological record of the slow slip environment.

2 Model Setup and Approach

Our model setup consists of a 4-km-wide by 20-km-long, visco-elasto-plastic shear zone (representing a cross-section through the subduction interface) bounded by two elastic plates that impose right-lateral shear at constant velocity (Figure 1). The low viscosity shear zone contains inclusions of varying sizes, aspect ratios, and distributions, intended to represent heterogeneous higher viscosity lenses (e.g. underplated mafic fragments). The model builds upon the approach outlined by Herrendörfer et al. (2018), which combines earthquake cycle simulations using a regularised Rate and State Friction (RSF) formulation (cf. Lapusta et al., 2000) with seismo-(thermo)-mechanical (STM) approaches developed by van Dinther et al. (2013). The STM component of the code is a continuum-based approach that simulates visco-elasto-plastic deformation in response to applied forces. The STM component is combined with an invariant form of rate-and-state-friction, including dynamic rupture propagation and seismic wave generation, applied to spontaneously-generated and evolving faults. An adaptive time-stepping routine allows fault slip velocities to be resolved over ~9 orders of magnitude (Herrendörfer et al., 2018).

Our primary interest is in the interplay between the lower viscosity matrix and higher-viscosity inclusions, and how their interactions modulate simulated event characteristics such as nucleation sites, fault plane geometries, slip velocities, moment-duration relationships, rupture propagation rates, recurrence intervals, and stress drops. To investigate this, our reference model implements a threshold shear zone viscosity (η_t) representing the frictional-viscous transition, with the static frictional yield strength defined as:

$$\tau_s = \mu\sigma_n, \tag{1}$$

and the threshold viscosity as:

$$\eta_t = \frac{\tau_s}{2\dot{\epsilon}} = \frac{\mu\sigma_n}{2\dot{\epsilon}}. \tag{2}$$

With the implementation of rate-and-state friction, the static stress (τ_s) is replaced with a regularized (Lapusta et al., 2000; Rice et al., 2001) and invariant (Herrendörfer et al., 2018) form of the velocity-dependent RSF formulation:

$$\tau_{II} = a\ P\ \ arcsinh\left[\frac{V_p}{2V_0}\exp\left(\frac{\mu_0 + b\ \ln\left(\frac{\theta V_0}{L}\right)}{a}\right)\right] \tag{3}$$

where τ_s is replaced by the second invariant of the stress tensor (τ_{II}), σ_n is replaced by the effective pressure P, $V_p = \epsilon_{II}2D$ (where D is the grid cell size) is the plastic slip velocity, V_0 is the reference slip velocity, μ_0 is the reference friction coefficient, L is the characteristic slip distance, a is the RSF direct effect, and b is the RSF evolution effect. b is described by the aging evolution law (e.g. J. Dieterich, 1994; Lapusta et al., 2000; Liu & Rice, 2005):

$$\dot{\theta} = 1 - \frac{V\theta}{L}. \tag{4}$$

An approximate nucleation size (h^*) is defined, above which simulated events start to propagate dynamically (cf. Rubin & Ampuero (2005)):

$$h^* = \frac{2}{\pi}\frac{GbL}{(b-a)^2 P_b(1-v)}, \tag{5}$$

where P_b is the effective pressure, G is the shear modulus and ν is Poisson's ratio.

The input model parameters are shown in Table 1. We assume a small effective pressure of 3.75 MPa, consistent with inferences of high fluid pressures and low effective normal stresses in subduction shear zones (e.g. Audet et al., 2009; Peacock et al., 2011; Taetz et al., 2018; Ujiie et al., 2018; Warren-Smith et al., 2019). The entire shear zone (inclusions and matrix) are implemented with the same elastic properties, velocity-weakening ($a-b$) and reference RSF parameters, and initial state. The forcing blocks outside the shear zone are set up with velocity strengthening conditions and high initial state. For these conditions, the threshold matrix viscosity is 10^{18} Pa·s and h^* is equal to 3.2 km. We assume the matrix deforms via linear viscous mechanisms, consistent with microstructural observations from rocks suggesting pressure-solution or diffusion-creep mechanisms are active in subduction shear zones (Behr & Platt, 2013; Fagereng & Den Hartog, 2017; Platt et al., 2018; Stöckhert,

Table 1. Model Parameters

Parameter	Symbol	Value
Shear modulus	G	30 GPa
Bulk Modulus	K	50 GPa
Poisson ratio	ν	0.25
Density	ρ	2700 kg/m^3
Shear wave speed	C_s	3.3 km/s
Shear zone width	W_s	4 km
Bulk shear zone strain rate	$\dot{\epsilon}$	1.5×10^{-12}/s
Initial mean stress	P_B	4 MPa
Gravity	g	9.8 m/s
Reference friction	μ_0	0.5
Reference slip velocity	V_0	4×10^{-9} m/s
Characteristic slip distance	L	.001 m
RSF direct effect	a	0.011
RSF evolution effect	b	0.017
Initial state	θ_i	Forcing block: $\frac{L}{V_0}$exp(40) s Shear zone: $\frac{L}{V_0}$exp(-1) s
Forcing block viscosity	η_b	1×10^{23} Pa·s
Clast viscosity	η_c	1×10^{22} Pa·s
Threshold viscosity	η_t	1×10^{18} Pa·s
Shear zone matrix viscosity	η_{sz}	.001-2000$\times\eta_t$
Clast spatial density	ρ_c	20-90%

2002; Wassmann & Stoeckhert, 2013). A viscosity gradient is implemented at the horizontal shear zone margins in an effort to limit interactions between propagating ruptures and model boundaries. Inclusions are implemented with a random size distribution such that their long dimensions can be close to, but are always less than the nucleation size. The location and aspect ratios of inclusions are varied randomly about a narrow distribution and inclusions are permitted to slightly overlap.

Model outputs include all physical parameters such as stress, strain rate, viscosity and velocity. For tracking transient slip events, we record the maximum velocity within the model domain for every timestep. Due to the gradual change of the slip velocity during seismic events, their durations were computed using a variable velocity threshold ($V_{threshold}$) defined as a function of the maximal slip velocity (V_{max}) recorded during each individual event. Since the maximum slip velocity is unknown *a-priori*, we integrated characteristics of all events for 14 different pre-defined thresholds (V_i) ranging from 10^{-8} to 10^{-1} m/s with 0.5 increment in the power exponent. The characteristic velocity threshold for each recorded event was then defined a *a-posteriori* as $V_{threshold} = V_i$ when $10^3 V_i < V_{max} < 10^{3.5} V_i$. Moments for each event were integrated for each V_i by accounting for all grid nodes slipping with slip rate $V_n > Vi$ as $M = \sum^t \left(dt \sum^{n,(V_n>V_i)} (V_n G) \sum^{n,(V_n>Vi)} (dx)^2 \right)$ where dt is the current time step, dx is the horizontal grid step and G is the shear modulus.

3 Model Results

3.1 Summary of General Model Behaviors

All models begin with a stage of shear zone loading in which strain rates progressively increase in the shear zone matrix and elastic strain accumulates in the higher viscosity clasts, with the timescale of this stage controlled by the Maxwell relaxation time (η/G). The visco-elastic deviatoric stress distributions that are set up in this initial stage are heterogeneous, with concentrations and shadows developed as a function of clast distribution and spatial density. Where stress concentrations exceed the frictional yield strength, plastic slip begins accumulating on localized slip zones that develop on both the margins and in the interior of clasts. For all model runs conducted near the threshold viscosity, the initial orientations of these failure planes are conjugate sets controlled by the static friction coefficient, consistent with Coulomb theory, with low values of μ_i generating planes oriented at lower angles to the shear zone walls (Fig. 2d-g). Local deflections of slip plane orientations do occur in some models near stress rotations adjacent to inclusions, however, leading to non-planar rupture geometries (e.g. Fig. 2e) (cf. Preuss et al., 2019).

The slip velocities on rupture planes initially grow exponentially as ruptures propagate due to the RSF direct effect. Once ruptures have initiated, they can propagate in either direction along their length. Whether ruptures will continue to propagate through the model domain depends on the local stresses at the rupture tip, which is the sum of the dynamic stresses associated with the rupture front itself and the heterogeneous background stresses set up within the shear zone. If a rupture tip migrates into a zone of relatively high stresses, the slip velocity and propagation velocity increases; whereas if the rupture tip migrates into regions of low stresses, the slip velocity decreases, and if stresses are low enough, the rupture arrests. In cases where a rupture reaches the nucleation size (cf. Eq. 5), it begins to propagate dynamically. Variations in rupture speed during dynamic rupture propagation can lead to generation of shear and pressure waves that radiate away from the slipping zone. The propagating ruptures produce regions of low state relative to the surrounding unslipped regions. Due to the short timescale of our model runs and the comparatively slow aging law, rupture planes persist as low state zones throughout the model duration such that eventually the initially high-viscosity inclusions (and in some cases the shear zone matrix) become cut by numerous low state fault planes.

3.2 Simplified two-inclusion models

To illustrate the general model behaviors in more detail, we first use simplified two-inclusion models. Figure 2 shows the initial conditions, model state, and maximum velocity as a function of timestep for two-inclusion models with different matrix viscosities and/or different friction coefficients. Figure 2c highlights the initial stress field in which, because of their higher viscosity with respect to the surrounding matrix, the inclusions are under compression and generate stress concentrations and shadows in the surrounding lower-viscosity matrix.

Figure 2d-g shows the rupture patterns for four different model runs after an arbitary number of timesteps (6500). For the threshold viscosity case (Fig. 2d), clasts are loaded to failure by surrounding viscous shear, but ruptures are generally confined to the clasts themselves, except where local stress concentrations around and between the clasts permit ruptures to propagate short distances into the matrix. This behavior illustrates the viscous damping (i.e. effectively velocity-strengthening) effect of the low viscosity matrix. Because the stresses in the model are always near the frictional yield strength, the slip velocities of intra-inclusion ruptures are slow (Fig. 2h) and all ruptures are quenched before they reach the critical nucleation size.

Figure 2e shows a model run in which the matrix viscosity is 10 times larger than η_t. Ruptures nucleate at stress concentrations on the inclusion margins and begin to prop-

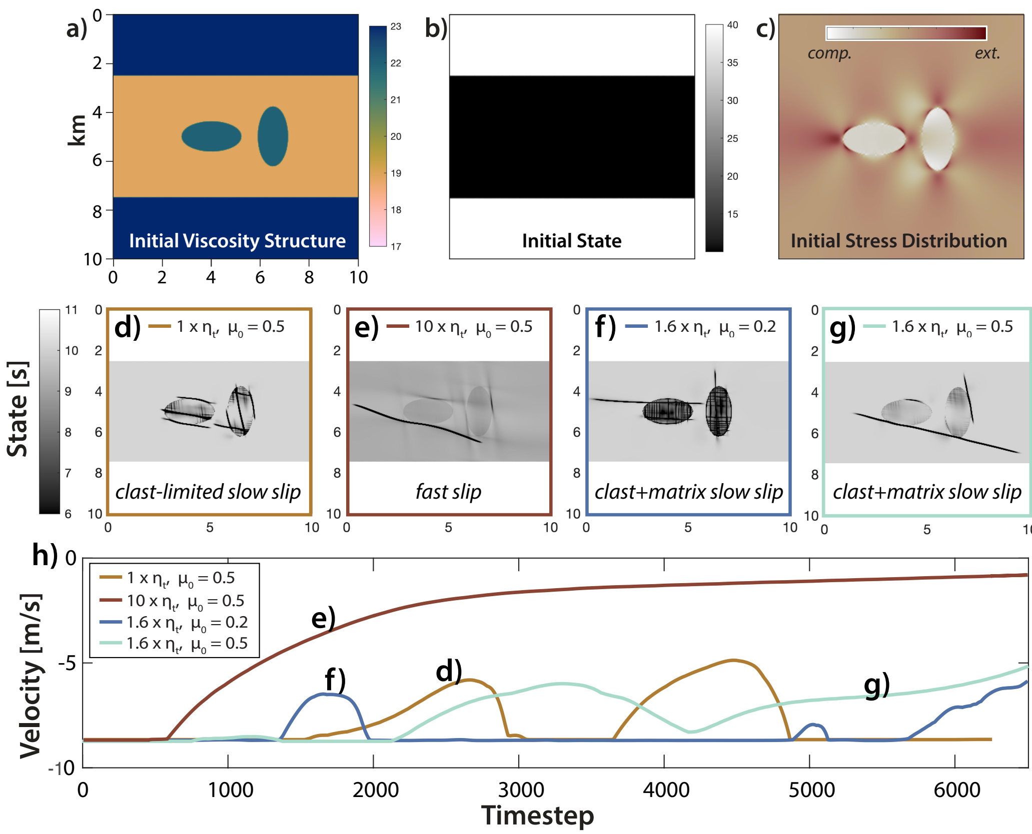

Figure 2. Initial conditions (a-c), model state (d-g), and velocity (h) as a function of timestep for simplified two-inclusion models with different matrix viscosities and/or different friction coefficients. See Section 3.2 for detailed description.

agate unhindered through the lower viscosity matrix. Although the rupture orientations in this regime are influenced by the model stress field, the slip velocities are not affected and velocities on these rupture planes grow exponentially toward the maximum of 0.1-1 m/s. This behavior ensues because the matrix viscosity, above the threshold value, sets up higher stress magnitudes in the shear zone, thus favoring fast frictional slip and allowing the ruptures to reach the nucleation size and propagate dynamically.

Figure 2f-g shows two model runs in which the matrix viscosity is slightly above the threshold value, but with different coefficients of friction. In this regime, ruptures can propagate through the matrix in regions of stress concentration, but they slip at slow velocities because the stress magnitudes ahead of the rupture tip are very close to the threshold value, and because the rupture tips occasionally propagate into stress shadows that lead to velocity decreases. The changes in μ_0 result in different orientations of ruptures, but the overall event patterns are similar. These two model runs show the potential for near-threshold models to develop ruptures of significant length that link multiple inclusions through the matrix across the model domain, but that nonetheless maintain slow slip velocities (Fig. 2h) due to low overall stresses and stress heterogeneity.

3.3 Multi-Inclusion Models

Here we focus on more complex multi-inclusion models in which only the matrix viscosity and the average spatial density of inclusions were varied; all other parameters remained constant as in Table 1. Figure 3 shows the initial viscosity, stress distributions at the onset of plastic yielding, and state at the end of the model run, for six example model cases with varying starting matrix viscosities and clast distributions. Figure 4 shows the event velocities through time for the same six model cases. We bin the models into three general categories based on shear zone matrix viscosity: above-threshold, near-threshold, and below-threshold models, and four categories of clast percentage (ρ_c): low ρ_c, medium ρ_c, high ρ_c, and clast-free.

3.3.1 Above-Threshold Models

Above-threshold models are classified as those in which the matrix viscosity is 100-2000 times the threshold viscosity. Because the viscosities in these models are too high to permit any significant viscous creep, the model behaviors are dominated by elastoplastic interactions and are insensitive to clast distributions and densities. Stresses build at the model corners near the imposed viscosity gradient as the clasts do not produce significant stress heterogeneity (Fig. 3a) and ruptures propagate at rates of 0.1-1 km/s horizontally along the shear zone boundary across the model domain (Fig. 4a). Model events approach maximum slip velocities (0.1-1 m/s, Fig. 4a) because of the stress magnitudes well above the frictional yield strength and the associated direct effect of RSF. Throughout the model runs, only one fault plane is active at any particular time, so the event patterns shown in Figure 4a reflect the true event recurrence interval. With time in the models, initial rupture planes are repeatedly occupied by high-velocity events that generate seismic waves that reverberate across the model domain. Because fast slip events dominate in these model runs, the events themselves are sometimes affected by propagation to the model boundaries and by interference from the propagating seismic waves as they reflect off of the non-absorbent model boundaries; this is an artifact of the model setup that explains some secondary low-velocity events recorded in these models, but does not substantially affect the overall rupture patterns.

3.3.2 Below-Threshold Models

Below-threshold models are those in which the viscosity of the shear zone matrix is 5-100× less than the threshold viscosity. For low to intermediate clast densities, these models do not generate sufficient stress concentrations to produce significant plastic yielding in

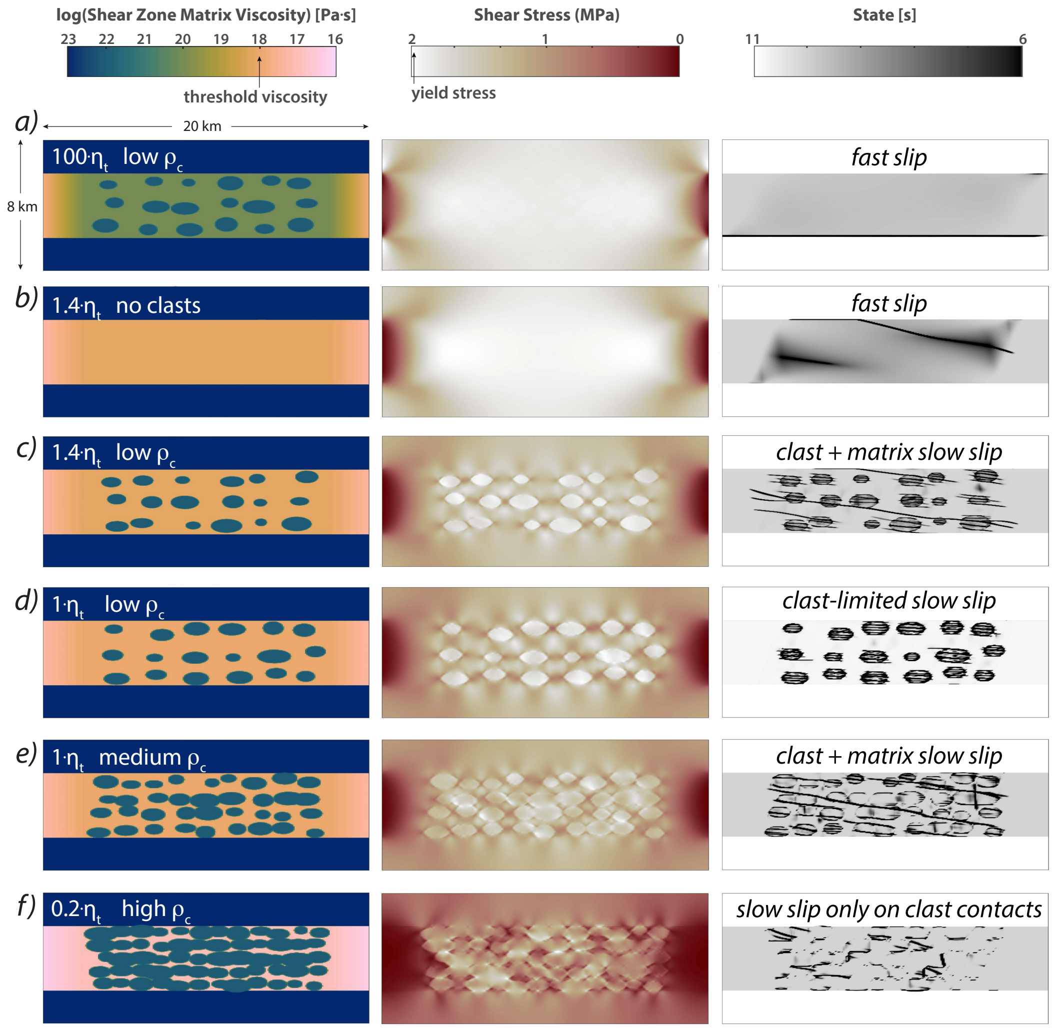

Figure 3. Initial conditions, initial stress state, and state at the end of the model run for 6 models with different matrix viscosities and different clast concentrations. Event velocities over time are shown for these same model runs in Figure 4. a) High matrix viscosity well above η_t leads to fast (cf. Fig. 4) slip events that propagate along the shear zone boundaries. b) Clast-free model just above η_t yields dominantly fast slip events that nucleate in the shear zone matrix and eventually propagate along shear zone boundaries. c) Same viscosity as in b) but with a low concentration of clasts. This leads to dominant slow slip (cf. Fig. 4) with several slip planes rupturing through the shear zone matrix. d-e) Models with viscosities at η_t but with different clast concentrations. Low ρ_c leads to clast-limited slow slip events whereas an increase in ρ_c leads to slow slip with ruptures that extend through the shear zone matrix. f) Below threshold viscosity model with high clast concentration. Slow-to-moderate velocity slip events are generated but only at direct contacts between clasts, after which the shear zone deforms at a steady state rate.

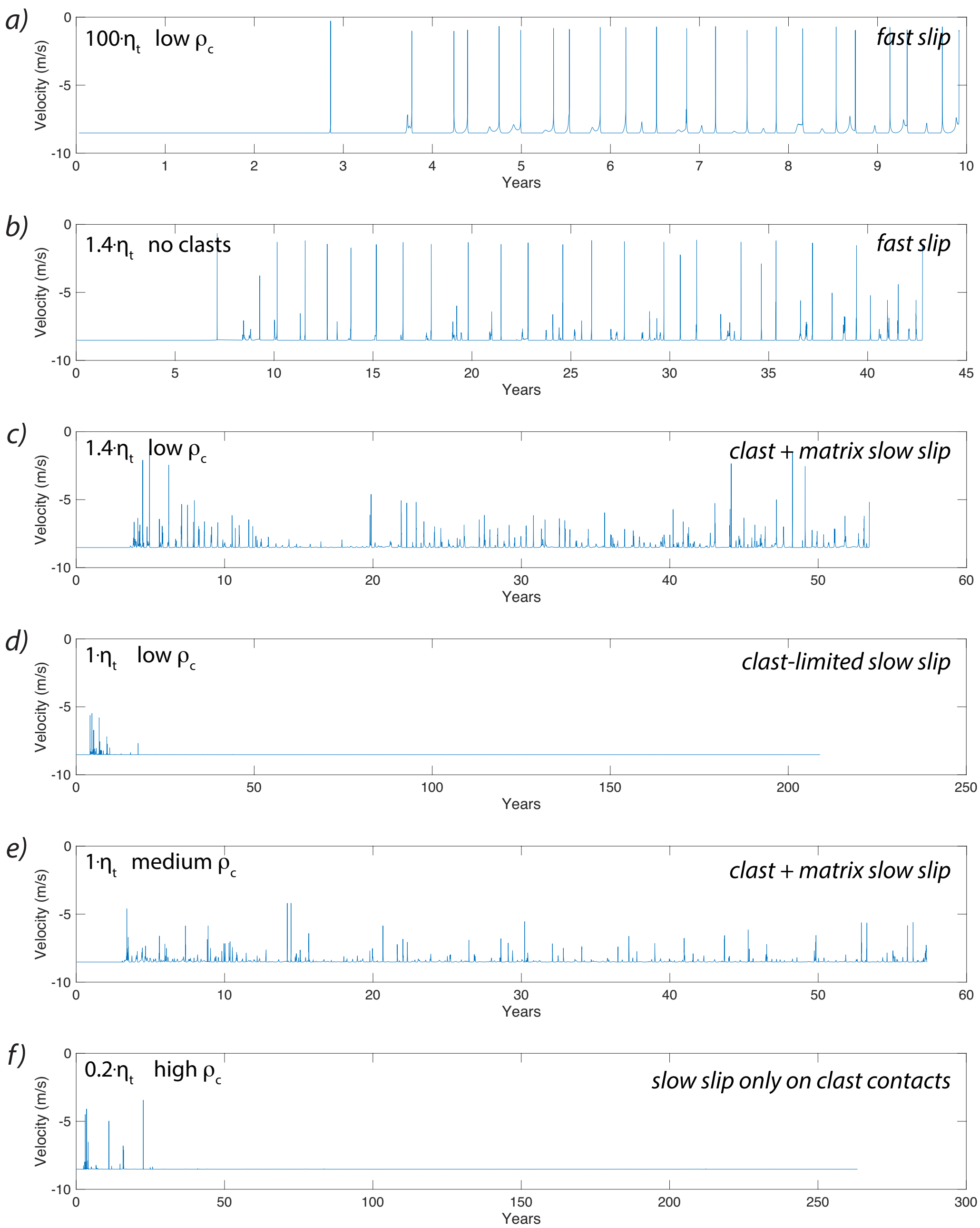

Figure 4. Maximum velocity over time for the models shown in Figure 3.

clasts, so no frictional failure or transient deformation occurs and the shear zone deforms at a constant steady-state strain rate. At high clast densities, however, some events are generated in the model. Figure 3f, for example, shows a model with a matrix viscosity that is 10x less than η_t, but with 70% clasts clustered to form a load-bearing framework. This model shows the development of stress concentrations at clast–clast and clast–shear-zone-wall contacts. This produces an early phase of small events with slow- to intermediate- slip velocities (Fig. 4f). The events only propagate along clast-clast or clast-shear zone interfaces but are immediately quenched when they reach viscous matrix regions due to the damping effect of the very low matrix viscosity. The high-stress contact points gradually become regions of low viscosity and low state, after which transient events are no longer generated as sufficient stress magnitudes are no longer attained. Unlike in the above-threshold models, several events can occur simultaneously in the 2D model domain, so the event patterns in Figure 4 represent only the maximum-velocity events occurring at any one time and therefore reflect a minimum recurrence interval.

3.3.3 Near-Threshold Models

Near-threshold models are defined as those in which the viscosity of the shear zone matrix is 1-10× greater than the threshold viscosity. Models in which the viscosity is equal to the threshold value and clast densities are low show nucleation of events in clasts and slow slip (averaging $\sim 10^{-7}$ m/s, Fig. 4c) along these rupture planes, but as in Figure 2d, the ruptures are quenched when they propagate into the surrounding matrix (Fig. 3c). Increasing clast densities in threshold models, or increasing the matrix viscosity to slightly above the threshold value (e.g. 1.1-1.4×), however, each have the effect of slightly elevating average stresses in the shear zone matrix, thus promoting through-going ruptures in some parts of the model domain. Figure 3d, for example, shows a model run in which the viscosity is still at the threshold value, but because the clast density is higher, some through-going rupture planes develop, linking the margins of multiple clasts, and at least one rupture surface propagates through most of the model domain at slow velocity. Similarly, Figure 3c shows a model case in which ρ_c is low, but because of the slightly above-threshold viscosity, events can propagate farther into the matrix, linking ruptures between high viscosity lenses, but still slipping at slow average velocities ($<10^{-2}$ m/s) and never reaching normal earthquake slip rates.

The maintenance of stress magnitudes very close to the frictional yield strength in near-threshold models also produces some behaviors through time that are not observed in other model types. For example, in many model runs, the propagation of ruptures into regions of the matrix that are only slightly below the frictional yield stress leads to dynamic triggering of nearby rupture surfaces that propagate in the same or the opposite direction as the initial rupture front (Video 1). Additionally, as in the below-threshold models, many events can occur simultaneously in the 2D model domain, so the event patterns in Figure 4 represent a minimum recurrence interval. Contrary to the above-threshold models, the propagation rates of ruptures in near-threshold models are much slower, ranging from ~ 0.1 to 20 km/day.

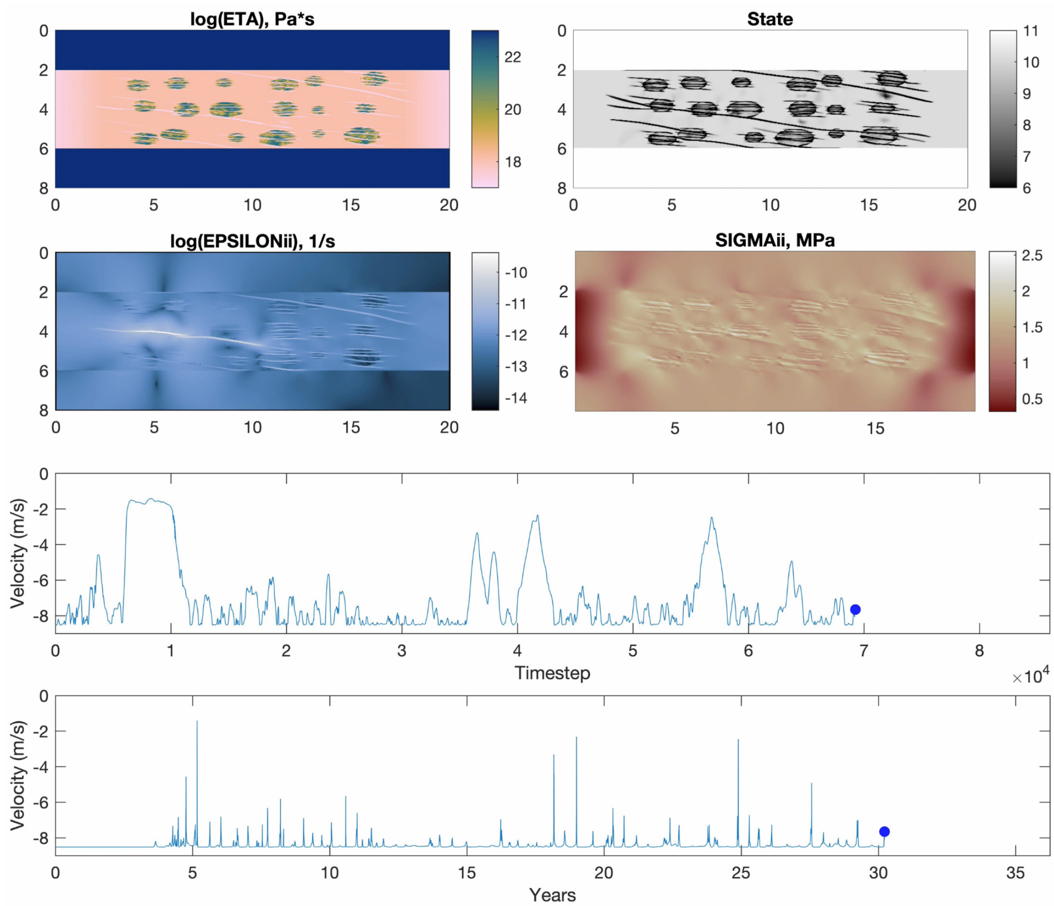

Video 1. Video of a near-threshold model with low clast concentration. The sequence begins with ruptures developing throughout the model domain only in clasts. These rupture planes eventually coalesce and link up across the shear zone matrix. At 30 seconds, a moderate-to-fast-velocity event nucleates and generates seismic waves that propagate through the model domain until 57 seconds. The rest of the model run shows repeated slow slip events that link clasts and matrix on single rupture planes. In several instances propagating ruptures trigger slip on nearby rupture surfaces, in both forward- and reverse-propagation directions.

The specific influence of stress heterogeneity, induced by the presence of clasts, on event slip velocity in near-threshold models can also be examined by comparing near-threshold models with and without clasts (Fig. 4b-c). Models in which the matrix viscosity is equal to the threshold value, but where no clasts are implemented do not generate events because no stress heterogeneity is present to push the model over the threshold stress toward frictional failure. This is in contrast to threshold models with clasts, which generate slow slip events due to failure within the clasts and subsequent quenching in the shear zone matrix (Fig. 4c-d). Models in which the matrix viscosity is slightly above the threshold value, with no clasts present, are dominated by moderate- to fast-velocity, regularly-recurring events (Fig. 4b) that characteristically propagate across the whole model domain (Fig. 3b)– the lack of stress heterogeneity prevents slip velocity perturbations from developing such that slip velocities continue to grow exponentially with increasing slip. This contrasts with the event patterns for models with the same matrix viscosity, but in which clasts are present, which are dominated by slow slip events with shorter (and more irregular) minimum recurrence times, and in which only some ruptures propagate as a single surface through the entire model domain (Fig. 4c).

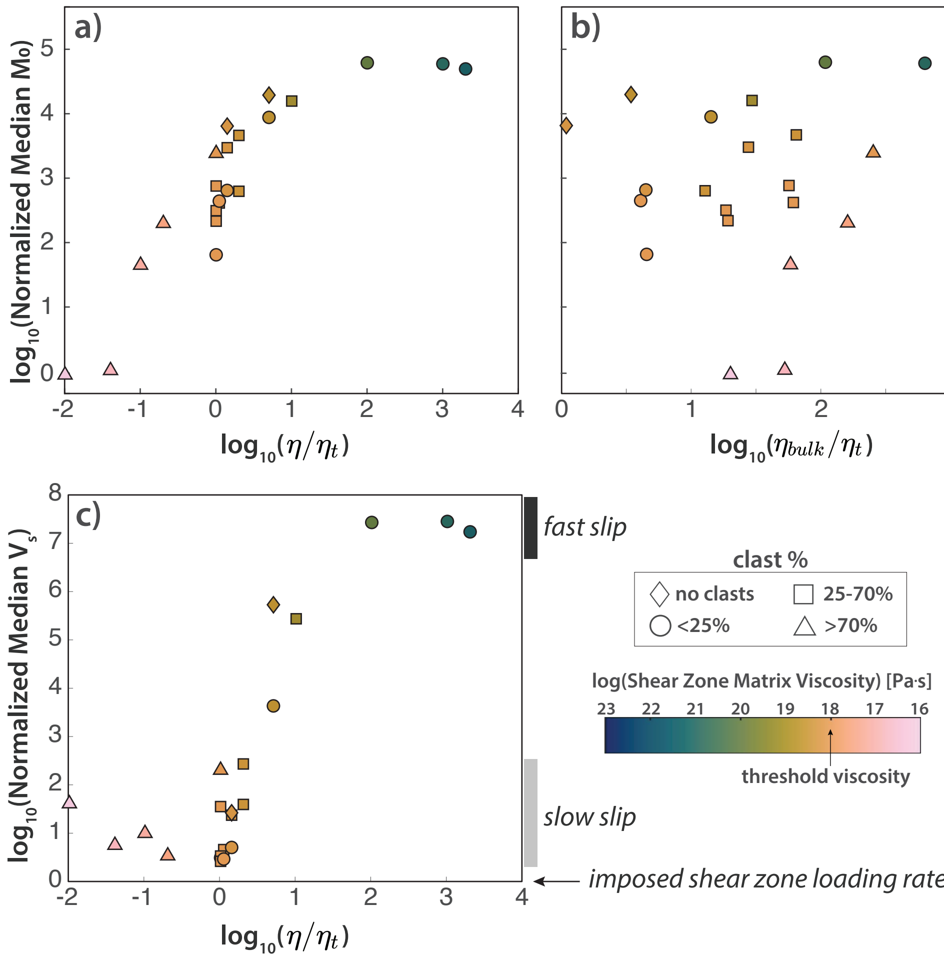

Figure 5. Normalized median moment and median event velocities as a function of matrix and bulk viscosity, with symbols representing clast distributions.

4 Model Event Statistics

Here we use the full suite of model runs to examine trends in transient event patterns as a function of shear zone viscosity and clast concentration, including median moments (normalized to the minimum model event size), and median event slip velocities (normalized to the imposed velocity across the shear zone) (Figure 5).

Figure 5a illustrates that there is a quasi-linear relationship i log-log space between the median moment for modeled events as a function of shear zone matrix viscosity, with higher moments associated with stronger shear zone matrices (Fig. 5a). This occurs because ruptures nucleating in clasts can propagate farther into the shear zone matrix when the matrix viscosity (and stress) is higher on average, thus producing longer rupture surfaces (cf. Section 3). The relationship appears to saturate at matrix viscosities ~100x the threshold viscosity because the stress magnitudes in these models are nearly everywhere above the frictional yield strength, so ruptures are never quenched in the matrix and therefore propagate across the full model domain.

Figure 5b indicates that the correlation between moment and viscosity does not apply in the case of the *bulk* viscosity of the shear zone; i.e. the bulk viscosity for shear zones with very low matrix viscosity, but high clast content is 1-2 orders of magnitude larger than threshold viscosity models with moderate clast contents, yet the median moment for events is still small. This emphasizes the importance of the intervening weak viscous matrix material in modulating slip behavior through its ability to damp nucleated ruptures, even when clast concentrations and bulk viscosities are high.

Figure 5c shows the correlation between matrix viscosity and median event slip velocity. Events for models at and below the threshold viscosity exhibit similar event slip velocities of up to 3 orders of magnitude larger than the imposed shear zone loading rate, whereas above-threshold models show faster median slip velocities with increasing matrix viscosity, again saturating at ∼100x the threshold viscosity.

We can also examine how our specific model parameters and associated transient event patterns scale with natural slow slip phenomena, by examining moment release patterns, stress drops, and moment-duration scaling (Fig. 6). Similar to what is shown in Figure 5a, Figure 6a shows a clear correlation between cumulative moment release over time and shear zone matrix viscosity. Furthermore, the plot demonstrates that above-threshold models (or those near-threshold models with higher clast contents) show very regular moment release over time, whereas near-threshold models with low clast contents exhibit an early phase of moment release associated with ruptures generated only in clasts, followed by a later phase of more regular moment release when ruptures coalescence to form planes that link up across the model domain. A more detailed analysis or comparison of recurrence intervals among model types is not appropriate here because the model setup tracks only the maximum velocity within the 2D model domain, whereas as noted in Section 3, near-threshold and below-threshold models commonly exhibit multiple events occurring simultaneously or in close succession. Additionally, in reality, event recurrence intervals are not only sensitive to plate boundary loading rates, but also to rates of fault healing (e.g. Fisher et al., 2019; Marone et al., 1995; McLaskey et al., 2012; Sibson, 1992), a poorly understood process that in our model framework would affect the time evolution of the state variable, but varying this parameter was beyond the scope of this study.

Figure 6b demonstrates that there is an overall positive relationship between the stress drop of modeled events and their moment magnitude (M_w), although the slope of this relationship appears to steepen for lower M_w. Stress drops for all modeled events range from less than ∼4 kPa to 2 MPa, with higher viscosity models exhibiting higher moment magnitudes (cf. Fig 5a-b) and larger stress drops. For modeled slow slip events in particular, stress drops range from ∼4-300 kPa, averaging ∼100 kPa.

In Figure 6c, the model event statistics are compared to the scaling relationships for slow slip versus regular earthquakes proposed by Ide et al. (2007). The majority of events in the models are slow events that form a narrow swath with a M≃4.5T scaling that in nature would be mostly seismically and geodetically undetectable. These are primarily events generated within clasts or at clast margins that propagate until they are quenched in the viscous matrix. As discussed in Section 3, below-threshold models with very high clast densities generate point-like stress concentrations along clast-clast contacts— the failure of these contacts produce small, but still slow slip events that extend downward in moment-duration space toward the region defined by very low frequency earthquakes (pink triangles in Fig. 6b). Ruptures in near-threshold and above-threshold models that are able to propagate from clasts into the matrix increase in both slip velocity and fault slip area, and are therefore drawn downward toward shorter durations and larger moments. Near-threshold model events with low to intermediate clast contents cluster around the slow slip scaling line, specifically overlapping with events characterized by Bletery et al. (2017), referred to as 'secondary slip fronts'. With increasing matrix viscosity, model events are drawn even farther toward shorter durations and greater moments such that they start to overlap with regular earthquake phenomena. This transition between the slow-slip scaling and regular earthquake scaling is a continuous transition as a function of matrix viscosity in our models;

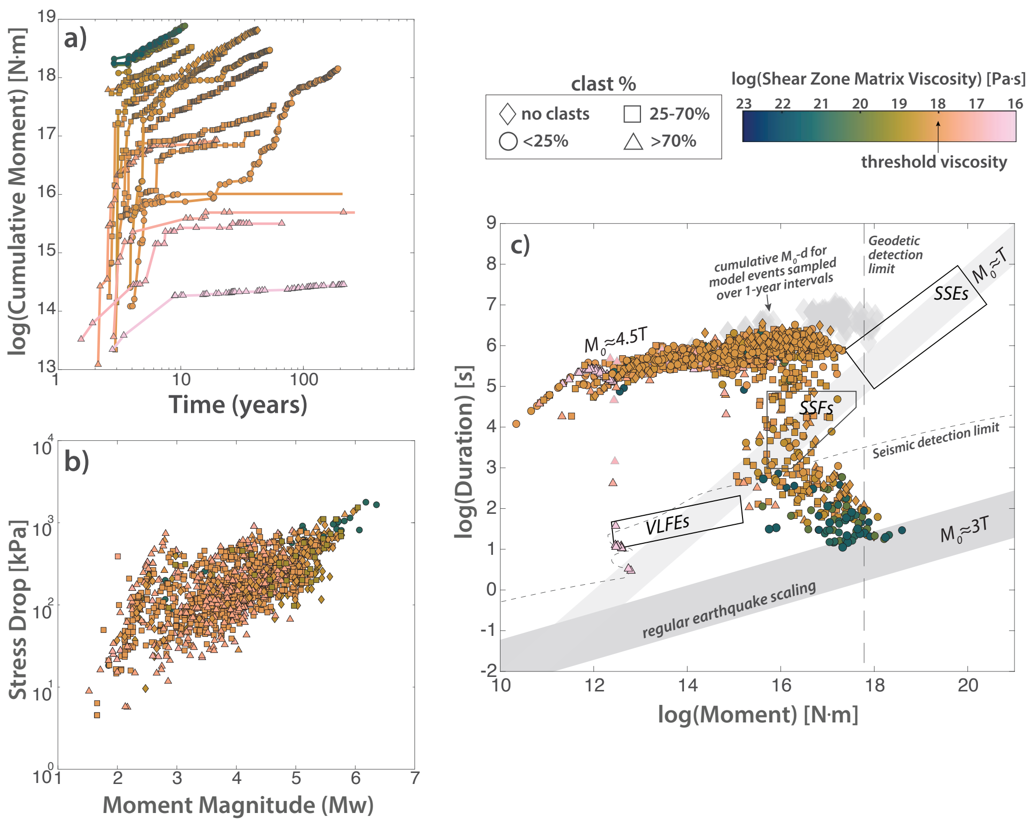

Figure 6. a) Cumulative moment release over time, b) computed stress drops as a function of moment magnitude and c) moment-duration statistics for modeled events, colored by viscosity and with symbols representing ρ_c.

i.e. we do not observe any gap in moment-duration space between slow slip and regular earthquakes (discussed further in Section 5).

Individual events in our models only partially overlap with the large seismic moments but long durations estimated for several natural slow slip events based on geodetic inversions. For example, our largest moment–longest duration events overlap significantly with slow slip associated with ETS events documented for Cascadia during the time period 2007-2017 (cf. Michel et al., 2019), but individual model events do not reach the larger moments and longer durations that have been documented for some events in Cascadia, and several in New Zealand, Mexico, Alaska and Japan (cf. Fig. 5 in Z. Peng & Gomberg, 2010). This is partly because the maximum moment in our models is limited by our choice of nucleation size ($h*$) and model domain length (itself limited by computational expense). However, model limitations aside, a growing body of observations from modern subduction zones suggest that slow slip events may comprise an amalgamation of multiple shorter-duration slip episodes (e.g. Bletery & Nocquet, 2020; Bletery et al., 2017; Frank et al., 2018). Our models potentially capture this behavior in cases where multiple ruptures trigger each other and are closely spaced in time (e.g. Video 1). To qualitatively examine this possibility from the perspective of modeled events, we calculated the cumulative moment for events sampled over random, 1-year intervals in one near-threshold model (grey diamonds in Fig. 6b). Events amalgamated in this way reach greater moments and longer durations that more closely overlap with the moment-duration statistics recorded in several modern subduction zones.

5 Discussion

5.1 Implications for Subduction Zone Transient Slip Patterns

In Figure 7 we plot the full suite of models as a regime diagram illustrating the expected seismic and transient slip behaviors as a function of matrix viscosity and clast percentage. The patterns of transient slip shown in this plot approximate the behavior of velocity-weakening, frictional-viscous systems for any threshold viscosity and clast size near the nucleation size, so are not strongly dependent on our specific choice of threshold viscosity, RSF parameters, or shear zone geometry or kinematics. The regime diagram thus provides a useful general framework for understanding how transient deformation may occur in heterogeneous frictional-viscous shear zones that define the deep roots of subduction megathrusts and other major plate boundary fault zones.

Although temperature was not explicitly implemented in our models, the three model types presented (above-threshold, near-threshold, and below-threshold) can be interpreted as three temperature endmembers along the plate interface because of the strong temperature dependence of viscosity. Above-threshold models represent low-temperature regions up-dip of the SSE zone, within the megathrust seismogenic region. Because the viscous yield strength is much higher than the frictional yield strength, subduction megathrust seismicity patterns in this regime have little to do with rock viscous properties, and their source physics are better captured by single-fault models in which frictional properties and/or geometries vary, as in numerous previous elastodynamic modeling studies (e.g. Ampuero & Rubin, 2008; J. H. Dieterich, 1992; Kaneko et al., 2008; Lapusta et al., 2000).

Near-threshold models, by definition, represent the frictional-viscous transition, and are thus intended to capture temperatures intermediate between those expected up-dip along the seismogenic megathrust and those expected down-dip in the zone of aseismic creep. The events in these models have several features in common with natural SSEs. This includes characteristically slow slip velocities that are ~1-3 orders of magnitude faster than the background plate rate, and, for our chosen model input parameters, rupture propagation rates of 0.1-20 km/day, and average stress drops in the range ~1-300 kPa. Events in near-threshold models also demonstrate that moment magnitudes approaching those derived

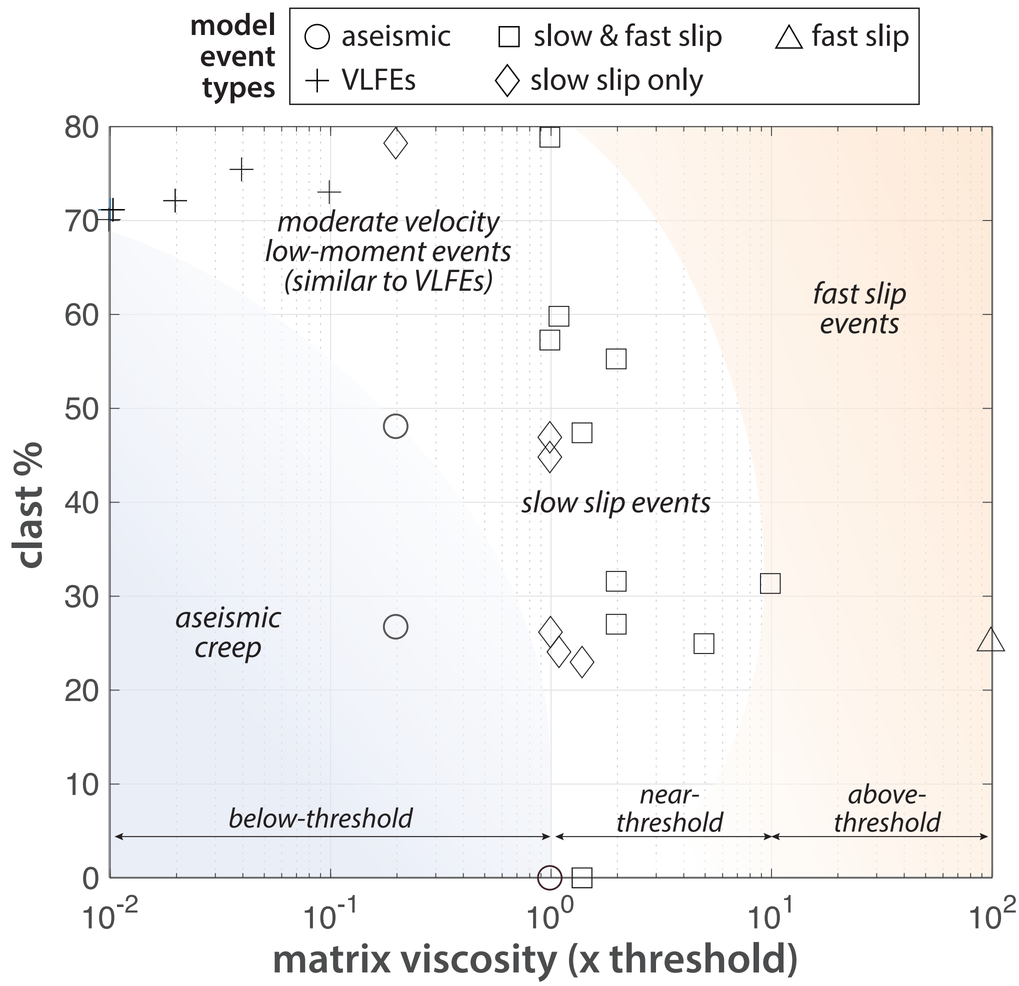

Figure 7. Regime diagram showing the expected slip behavior as a function of matrix viscosity and clast concentration.

geodetically from natural slow slip events can be produced through summation of multiple slip events within the 2D model domain and/or through single rupture surfaces that fail in close succession over time (Fig. 6). The interaction of ruptures within these models, including triggered events that propagate away from the main rupture front, resembles observations of tremor migrations in slow slip events (e.g. Bletery et al., 2017; Ghosh et al., 2010; Hawthorne et al., 2016; Obara et al., 2012; Y. Peng et al., 2015; Rubin & Armbruster, 2013).

With increasing viscosity above the threshold viscosity, the models show a progressive transition toward faster slip events, with some exhibiting intermediate slip velocities or mixed slow and fast slip. The models thus do not support a fundamental change in mechanism between fast and slow slip, but instead suggest a progressive decrease (updip)/increase (downdip) in the velocity-strengthening effects of viscous creep. The models predict that the region of the interface between the seismogenic megathrust and the dominantly slow slip zone should exhibit intermediate-velocity slip events that are seismically detectable. Very few natural events matching the moment-duration values expected for this viscosity range have been documented, however, so this reflects a potential discrepancy between our model predictions and natural observations. However, several studies have questioned the idea that slow slip and regular earthquakes obey different scaling relationships, and suggest a continuum between slow slip and regular earthquake fault slip modes (Frank & Brodsky, 2019; Gomberg et al., 2016; Hulbert et al., 2019; Leeman et al., 2016; Z. Peng & Gomberg, 2010), consistent with our model results.

Models in which the viscosity of the shear zone matrix is less than the threshold viscosity are potentially representative of conditions of increasing temperature at the downdip extent of the SSE zone and the transition to aseismic creep. Below-threshold models with very high clast contents are the only models to produce small-magnitude, moderately slow-velocity events that for our input model parameters resemble very low frequency earthquakes (Figs. 6,7). VLFEs, along with low frequency earthquakes, are commonly interpreted to compose the tectonic tremor signals that accompany slow slip (Ito et al., 2007; Katsumata & Kamaya, 2003; Obara, 2002; Rogers & Dragert, 2003; Shelly et al., 2006). Tremor is most commonly observed on the deeper sections of the subduction plate interface, whereas several recent observations suggest that there is a gap, where only long-term slow slip events are observed, located between the megathrust seismogenic zone and deeper zones of episodic tremor and slow slip (e.g. Kato et al., 2010; Rousset et al., 2017; Takagi et al., 2016). This gap is consistent with the observation in our models that VLFE-like events are only produced where the shear zone matrix viscosity is 1-2 orders of magnitude below the threshold viscosity (e.g. at higher temperature conditions of the interface corresponding to deeper depths). Although our models do not explicitly capture this, in the context of our model framework, combined episodic tremor and slow slip may represent slow slip events propagating from near-threshold-viscosity regions into clast-rich domains that contain pockets of lower viscosity material and that are tremorgenic.

5.2 Comparisons to the Geologic Record

In addition to matching some of the measured geodetic and seismic characteristics of slow slip events, several aspects of our models also resemble features preserved in exhumed rocks. As discussed in Section 1, many exhumed subduction shear zones from the deep interface show evidence for strong viscosity contrasts in the form of rigid blocks embedded in a viscous matrix (e.g. Angiboust et al., 2013, 2011b; Bebout & Barton, 2002; Kotowski & Behr, 2019; Marroni et al., 2009; Rad et al., 2005; Scarsi et al., 2018; Tarling et al., 2019; Ukar & Cloos, 2019). Experimental flow laws for subduction related materials suggest that viscosity contrasts can be up to 4 orders of magnitude for pressure-temperature conditions representative of the downdip megathrust (cf. Fig. 2 in Behr & Becker, 2018). Additionally, different spatial distributions of rigid clasts may be expected not only due to differing amounts of subducted mafic components, but also (especially in the case of warm subduction zones) different degrees of dehydration and metamorphism to form dry eclogite or amphibolite, which are rheologically hardened metamorphic rocks that enhance viscosity contrasts (Behr et al., 2018; Yamato et al., 2019). Several exhumed shear zones furthermore show evidence that the frictional yield strength in clasts was locally exceeded even near peak subduction depths, with clasts exhibiting both tensile and shear fractures that preserve high pressure mineral assemblages (Angiboust et al., 2011b; Bukała et al., 2020; Kotowski & Behr, 2019; Taetz et al., 2018). Some studies have also described evidence for continuation of structures nucleated in clasts into the surrounding dominantly viscously deformed matrix; whereas others highlight a cyclical interplay between brittle veining and viscoplastic slip on weak matrix cleavage planes (Fagereng et al., 2010; Kotowski & Behr, 2019; Platt et al., 2018; Ujiie et al., 2018).

Geologic features described above closely resemble the fracture sets and weak slip planes that develop as low state plastic slip zones within our models (Fig. 3). However, block-in-matrix structures and associated faults sets in subduction melange belts are most commonly documented at scales less than 10-100 meters due to limitations in the areas of geologic exposure. Thus, a persistent open question has been whether these types of structures could scale up to produce the large magnitudes characteristic of modern SSEs. Our models indicate that this upscaling is very likely to occur at conditions near the frictional-viscous transition at moderate clast concentrations, and that it can occur not only through linkages of single rupture surfaces from clast to clast through the matrix, but also through simultaneous or cascading failure of multiple triggered rupture surfaces within a finite-width shear zone (cf. Video 1). Our models thus support the idea that observations from individual melange outcrops are one length-scale of an approximately fractal system, that mimic the deformation processes occurring in multi-kilometer-scale (relevant to slow slip) 'mega-melange' belts consisting of rheologically heterogeneous underplated terranes (cf. Behr & Bürgmann, 2021).

5.3 Similarities and Differences to Other Frictional-Viscous Models

Ando et al. (2012) and Nakata et al. (2011) explored rupture dynamics of LFEs and VLFEs simulated for a 2D fault plane with a prescribed slow slip front propagating through heterogeneous patches of contrasting viscous and frictional (velocity-weakening vs. strengthening) properties. Rupture propagation in these models was governed by a viscous damping term such that stress transmission between heterogeneous patches was stifled by low background viscosities and/or low patch distributions. Skarbek et al. (2012) similarly examined slip behaviors for RSF models with alternating velocity-weakening and strengthening patches, varying both the $a - b$ parameters and the patch distributions. More recently, Lavier et al. (2021) explored the role of brittle-ductile interactions in finite-width shear zones, simulating ductile regions by matching velocity-strengthening frictional properties to variations in viscosity. Each of these model frameworks predicted a transition in rupture behavior from elastodynamic to slow slip, similar to what we observe here. In the purely elastic, one-dimensional model case of Skarbek et al. (2012), the transition from elastodynamic slip to slow slip was more abrupt and the range over which slow slip events could be expected was comparatively narrow. In the case of Lavier et al. (2021), velocity-neutral conditions in the ductile matrix are $\sim$equivalent to our threshold viscosity models, whereas increasing velocity-strengthening conditions simulates decreasing matrix viscosity. Their models produced behaviors similar to our below-threshold models shown in Figure 7, with aseismic creep dominating at low clast concentrations, transitioning to transient slip events when clast concentrations are increased to between 45 and 80% (cf. Figure 4c in Lavier et al. (2021)). In the case of our models, however, these transitions in slip style can be generated simply by varying matrix viscosity, with no variations in the velocity-dependent frictional properties within the shear zone required.

Visco-plastic models conducted in a study by Beall et al. (2019) also have some aspects in common with our below-threshold, high-clast-distribution models. Similar to their observations and previous work on granular materials (Daniels & Hayman, 2008; Hayman et al., 2011; Reber et al., 2015), we see the development of force chains extending across the model domain when clast densities are greater than ∼50% (cf. Figure 3e-f). Beall et al. (2019) suggested that the fracturing process in clast-rich shear zones may lead to switches from subduction zone 'jamming', in which clasts control the bulk strain rate, to periods of elevated strain rates localized in intervening weak viscous matrix regions after clast fracture, perhaps consistent with slow slip velocities. Our models suggest that the fracture process itself in jammed, high-viscosity-contrast shear zones may create seismicity that resembles very low frequency earthquakes, but that once these fractures have been generated throughout the model domain, the shear zone accommodates the imposed plate velocity by viscous creep at steady state. Incorporation of fracture healing processes could result in a regular oscillation of this process, however, potentially supporting the model proposed by Beall et al. (2019). However, our models also predict viscously-damped, yet still frictional slow slip, even in cases where the matrix viscosity (and associated viscous strain rate) is not particularly low and where clast concentrations are not high enough for clasts to directly interact; thus our models predict a wider range of conditions of both viscosity and clast concentration where slow slip may be anticipated (Fig. 7).

Our results are also consistent with previous models that emphasize the potential for frictional-viscous interactions to modulate event slip velocities, and for slow slip events to occur near the brittle-ductile or frictional-viscous transition in subduction environments (e.g. Goswami & Barbot, 2018), even in the absence of discretely implemented heterogeneities. Recent models by Petrini et al. (2020), for example, suggested predominant development of slow slip events at the downdip limit of the megathrust in a zone of prescribed gradually decreasing matrix viscosity. Above and below this transitional zone, respectively, seismic ruptures and aseismic slip emerged; and the moment-duration distributions computed by Petrini et al. (2020) bear several similarities with our results, despite implementation of quite different constitutive relationships.

Overall, a primary advantage to our model framework is the incorporation of a finite-width shear zone, which allows analysis of how spontaneously-generated, geometrically complex, rupture surfaces (e.g. similar to those observed in the rock record) may interact with each other, and how they may scale up to resemble a slow slip event (e.g. similar to those recorded using geodetic methods in active fault zones). There are also several limitations to the current model setup, however, that could pave the way for future developments, including exploration of realistic temperature and pressure gradients and shear heating, dynamic pressure and pore fluid pressure evolution, power law viscosity or viscous anisotropy effects, time evolution of the state variable to simulate fault healing processes, and effects of simultaneously varying frictional and viscous properties.

6 Conclusions

We show that models simulating earthquakes and transient slip events in heterogeneous viscoelastoplastic shear zones resembling subduction 'mega-melange' belts can reproduce several key aspects of natural slow slip and tremor phenomena, including matching slip velocities, propagation rates, and stress drops. For conditions near the frictional-viscous transition, the viscous component of these shear zones, and the stress heterogeneity set up by the presence of rigid clasts, set a 'speed limit' for earthquake ruptures such that they slip and propagate at velocities similar to natural slow slip events, despite constant velocity-weakening frictional properties. The viscous component simultaneously permits the transmission of slow slip from clast to clast, allowing slow ruptures to propagate substantial distances, even in cases where clasts are widely spaced— this potentially reconciles how slip planes observed at the outcrop scale by geologists may scale up to achieve hundred kilometer scales implied by geodetic inversions of slow slip events. Additionally, the implementation of a finite-width shear zone allows us to observe coalescence, triggering and reverse-propagation among multiple rupture surfaces within a thicker elevated-slip-rate zone, also consistent with emerging observations of slow slip as clusters of multiple slip transients. If our model framework of slow slip representing fault plane interactions within a finite-width shear zone is correct, it implies that estimated moments and recurrence intervals from natural slow slip and tremor events do not necessarily represent repeated failure of a single rupture plane, but instead may reflect multiple rupture planes slipping simultaneously or cascading through the width of a subduction interface shear zone.

Acknowledgments

This research was funded by an ERC Starting Grant (S-SIM, grant no. 947659) awarded to W.M.Behr and by an Swiss National Science Foundation grant awarded to T. Gerya (grant no. 200021-192296). WM Behr acknowledges several helpful discussions of the manuscript content with Thorsten Becker. All model images utilized the perceptually uniform colormaps from Crameri (2018). Data for model input parameters and videos of exemplary model runs will be made available on the ETH Research Collection data repository upon publication of this manuscript.

References

Agard, P., Plunder, A., Angiboust, S., Bonnet, G., & Ruh, J. (2018). The subduction plate interface: rock record and mechanical coupling (from long to short timescales). *Lithos*, *320*, 537–566.

Ampuero, J.-P., & Rubin, A. M. (2008). Earthquake nucleation on rate and state faults – aging and slip laws. *Journal of Geophysical Research*, *113*(B1).

Ando, R., Takeda, N., & Yamashita, T. (2012). Propagation dynamics of seismic and aseismic slip governed by fault heterogeneity and newtonian rheology. *Journal of Geophysical Research: Solid Earth*, *117*(B11).

Angiboust, S., Agard, P., De Hoog, J., Omrani, J., & Plunder, A. (2013). Insights on deep, accretionary subduction processes from the sistan ophiolitic "mélange"(eastern iran). *Lithos*, *156*, 139–158.

Angiboust, S., Agard, P., Raimbourg, H., Yamato, P., & Huet, B. (2011a). Subduction interface processes recorded by eclogite-facies shear zones (monviso, w. alps). *Lithos*, *127*(1-2), 222–238.

Angiboust, S., Agard, P., Raimbourg, H., Yamato, P., & Huet, B. (2011b). Subduction interface processes recorded by eclogite-facies shear zones (monviso, w. alps). *Lithos*, *127*(1-2), 222–238.

Audet, P., Bostock, M. G., Christensen, N. I., & Peacock, S. M. (2009). Seismic evidence for overpressured subducted oceanic crust and megathrust fault sealing. *Nature*, *457*(7225), 76–78.

Audet, P., & Bürgmann, R. (2014). Possible control of subduction zone slow-earthquake periodicity by silica enrichment. *Nature*, *510*(7505), 389–392.

Audet, P., & Kim, Y. (2016). Teleseismic constraints on the geological environment of deep episodic slow earthquakes in subduction zone forearcs: A review. *Tectonophysics*, *670*, 1–15.

Audet, P., & Schaeffer, A. J. (2018). Fluid pressure and shear zone development over the locked to slow slip region in cascadia. *Science Advances*, *4*(3), eaar2982.

Beall, A., Fagereng, Å., & Ellis, S. (2019). Fracture and weakening of jammed subduction shear zones, leading to the generation of slow slip events. *Geochemistry, Geophysics, Geosystems*, *20*(11), 4869–4884.

Bebout, G. E., & Barton, M. D. (2002). Tectonic and metasomatic mixing in a high-t, subduction-zone mélange—insights into the geochemical evolution of the slab–mantle interface. *Chemical Geology*, *187*(1-2), 79–106.

Beeler, N. M. (2009). Constructing constitutive relationships for seismic and aseismic fault slip. *Mechanics, Structure and Evolution of Fault Zones*, 1775–1798.

Behr, W., & Becker, T. W. (2018). Sediment control on subduction plate speeds. *Earth and Planetary Science Letters*, *502*, 166–173.

Behr, W., & Bürgmann, R. (2021). Whats down there? the structures, materials and environment of deep-seated slow slip and tremor. *Phil. Trans. Roy. Soc.*, *379*.

Behr, W., Kotowski, A. J., & Ashley, K. T. (2018). Dehydration-induced rheological heterogeneity and the deep tremor source in warm subduction zones. *Geology*, *46*(5), 475–478.

Behr, W., & Platt, J. (2013). Rheological evolution of a mediterranean subduction complex. *Journal of Structural Geology*, *54*, 136–155.

Beroza, G. C., & Ide, S. (2011). Slow earthquakes and nonvolcanic tremor. *Annual Review of Earth and Planetary Sciences*, *39*(1), 271–296.

Bletery, Q., & Nocquet, J.-M. (2020). Slip bursts during coalescence of slow slip events in cascadia. *Nature Communications*, *11*(1).

Bletery, Q., Thomas, A. M., Hawthorne, J. C., Skarbek, R. M., Rempel, A. W., & Krogstad, R. D. (2017). Characteristics of secondary slip fronts associated with slow earthquakes in cascadia. *Earth and Planetary Science Letters*, *463*, 212–220.

Bukała, M., Barnes, C., Jeanneret, P., Hidas, K., Mazur, S., & Almqvist, B. (2020). Ko smi nska k, klonowska i, ˇsurka j and majka j (2020) brittle deformation during eclogitization of early paleozoic blueschist. front. *Front. Earth Sci*, *8*, 594453.

Calvert, A. J. (1996). Seismic reflection constraints on imbrication and underplating of the northern cascadia convergent margin. *Canadian Journal of Earth Sciences*, *33*(9), 1294–1307.

Calvert, A. J., Bostock, M. G., Savard, G., & Unsworth, M. J. (2020). Cascadia low frequency earthquakes at the base of an overpressured subduction shear zone. *Nature Communications*, *11*(1).

Chen, K. H., Tai, H.-J., Ide, S., Byrne, T. B., & Johnson, C. W. (2018). Tidal modulation and tectonic implications of tremors in taiwan. *Journal of Geophysical Research: Solid Earth*, *123*(7), 5945–5964.

Cloos, M., & Shreve, R. L. (1988). Subduction-channel model of prism accretion, melange formation, sediment subduction, and subduction erosion at convergent plate margins: 2. implications and discussion. *Pure and Applied Geophysics*, *128*(3), 501–545.

Condit, C. B., Guevara, V. E., Delph, J. R., & French, M. E. (2020). Slab dehydration in warm subduction zones at depths of episodic slip and tremor. *Earth and Planetary Science Letters*, *552*, 116601.

Cowan, D. S. (1985). Structural styles in mesozoic and cenozoic mélanges in the western cordillera of north america. *Geological Society of America Bulletin*, *96*(4), 451–462.

Crameri, F. (2018). Geodynamic diagnostics, scientific visualisation and staglab 3.0. *Geoscientific Model Development*, *11*(6), 2541–2562.

Daniels, K. E., & Hayman, N. W. (2008). Force chains in seismogenic faults visualized with photoelastic granular shear experiments. *Journal of Geophysical Research: Solid Earth*, *113*(B11).

Delph, J. R., Levander, A., & Niu, F. (2018). Fluid controls on the heterogeneous seismic characteristics of the cascadia margin. *Geophysical Research Letters*, *45*(20).

Dieterich, J. (1994). A constitutive law for rate of earthquake production and its application to earthquake clustering. *Journal of Geophysical Research: Solid Earth*, *99*(B2), 2601–2618.

Dieterich, J. H. (1979). Modeling of rock friction: 1. experimental results and constitutive equations. *Journal of Geophysical Research*, *84*(B5), 2161.

Dieterich, J. H. (1992). Earthquake nucleation on faults with rate-and state-dependent strength. *Tectonophysics*, *211*(1-4), 115–134.

Fagereng, Å. (2011). Frequency-size distribution of competent lenses in a block-in-matrix mélange: Imposed length scales of brittle deformation? *Journal of Geophysical Research*, *116*(B5).

Fagereng, Å., & Den Hartog, S. A. (2017). Subduction megathrust creep governed by

pressure solution and frictional–viscous flow. *Nature Geoscience*, *10*(1), 51–57.
Fagereng, Å., Hillary, G. W., & Diener, J. F. (2014). Brittle-viscous deformation, slow slip, and tremor. *Geophysical Research Letters*, *41*(12), 4159–4167.
Fagereng, Å., Remitti, F., & Sibson, R. H. (2010). Shear veins observed within anisotropic fabric at high angles to the maximum compressive stress. *Nature Geoscience*, *3*(7), 482–485.
Fagereng, Å., & Sibson, R. H. (2010). Mélange rheology and seismic style. *Geology*, *38*(8), 751–754.
Festa, A., Pini, G. A., Dilek, Y., & Codegone, G. (2010). Mélanges and mélange-forming processes: a historical overview and new concepts. *International Geology Review*, *52*(10-12), 1040–1105.
Fisher, D., & Byrne, T. (1987). Structural evolution of underthrusted sediments, kodiak islands, alaska. *Tectonics*, *6*(6), 775–793.
Fisher, D., Smye, A., Marone, C., van Keken, P., & Yamaguchi, A. (2019). Kinetic models for healing of the subduction interface based on observations of ancient accretionary complexes. *Geochemistry, Geophysics, Geosystems*, *20*(7), 3431–3449.
Frank, W. B., & Brodsky, E. E. (2019). Daily measurement of slow slip from low-frequency earthquakes is consistent with ordinary earthquake scaling. *Science advances*, *5*(10), eaaw9386.
Frank, W. B., Rousset, B., Lasserre, C., & Campillo, M. (2018). Revealing the cluster of slow transients behind a large slow slip event. *Science advances*, *4*(5), eaat0661.
Ghosh, A., Vidale, J. E., Sweet, J. R., Creager, K. C., Wech, A. G., Houston, H., & Brodsky, E. E. (2010). Rapid, continuous streaking of tremor in cascadia. *Geochemistry, Geophysics, Geosystems*, *11*(12).
Gomberg, J., Wech, A., Creager, K., Obara, K., & Agnew, D. (2016). Reconsidering earthquake scaling. *Geophysical Research Letters*, *43*(12), 6243–6251.
Goswami, A., & Barbot, S. (2018). Slow-slip events in semi-brittle serpentinite fault zones. *Scientific reports*, *8*(1), 1–11.
Grigull, S., Krohe, A., Moos, C., Wassmann, S., & Stöckhert, B. (2012). "order from chaos": a field-based estimate on bulk rheology of tectonic mélanges formed in subduction zones. *Tectonophysics*, *568*, 86–101.
Hansen, R. T. J., Bostock, M. G., & Christensen, N. I. (2012). Nature of the low velocity zone in cascadia from receiver function waveform inversion. *Earth and Planetary Science Letters*, *337-338*, 25–38.
Hawthorne, J. C., Bostock, M. G., Royer, A. A., & Thomas, A. M. (2016). Variations in slow slip moment rate associated with rapid tremor reversals in cascadia. *Geochemistry, Geophysics, Geosystems*, *17*(12), 4899–4919.
Hawthorne, J. C., & Rubin, A. M. (2013). Laterally propagating slow slip events in a rate and state friction model with a velocity-weakening to velocity-strengthening transition. *Journal of Geophysical Research: Solid Earth*, *118*(7), 3785–3808.
Hayman, N. W., Ducloué, L., Foco, K. L., & Daniels, K. E. (2011). Granular controls on periodicity of stick-slip events: kinematics and force-chains in an experimental fault. *Pure and applied geophysics*, *168*(12), 2239–2257.
Hayman, N. W., & Lavier, L. L. (2014). The geologic record of deep episodic tremor and slip. *Geology*, *42*(3), 195–198.
Herrendörfer, R., Gerya, T., & van Dinther, Y. (2018). An invariant rate- and State-Dependent friction formulation for viscoeastoplastic earthquake cycle simulations. *Journal of Geophysical Research: Solid Earth*, *123*(6), 5018–5051.
Hulbert, C., Rouet-Leduc, B., Johnson, P. A., Ren, C. X., Rivière, J., Bolton, D. C., & Marone, C. (2019). Similarity of fast and slow earthquakes illuminated by machine learning. *Nature Geoscience*, *12*(1), 69–74.
Ide, S., Beroza, G. C., Shelly, D. R., & Uchide, T. (2007). A scaling law for slow earthquakes. *Nature*, *447*(7140), 76–79.
Im, K., Saffer, D., Marone, C., & Avouac, J.-P. (2020). Slip-rate-dependent friction as a

universal mechanism for slow slip events. *Nature Geoscience*, *13*(10), 705–710.

Ito, Y., Obara, K., Shiomi, K., Sekine, S., & Hirose, H. (2007, January). Slow earthquakes coincident with episodic tremors and slow slip events. *Science*, *315*(5811), 503–506.

Kaneko, Y., Lapusta, N., & Ampuero, J.-P. (2008). Spectral element modeling of spontaneous earthquake rupture on rate and state faults: Effect of velocity-strengthening friction at shallow depths. *Journal of Geophysical Research*, *113*(B9).

Kato, A., Iidaka, T., Ikuta, R., Yoshida, Y., Katsumata, K., Iwasaki, T., … Hirata, N. (2010). Variations of fluid pressure within the subducting oceanic crust and slow earthquakes. *Geophysical Research Letters*, *37*(14).

Katsumata, A., & Kamaya, N. (2003). Low-frequency continuous tremor around the moho discontinuity away from volcanoes in the southwest japan. *Geophysical Research Letters*, *30*(1), 20–21.

Kotowski, A. J., & Behr, W. (2019). Length scales and types of heterogeneities along the deep subduction interface: Insights from exhumed rocks on syros island, greece. *Geosphere*, *15*(4), 1038–1065.

Lapusta, N., Rice, J. R., Ben-Zion, Y., & Zheng, G. (2000). Elastodynamic analysis for slow tectonic loading with spontaneous rupture episodes on faults with rate- and state-dependent friction. *Journal of Geophysical Research: Solid Earth*, *105*(B10), 23765–23789.

Lavier, L. L., Tong, X., & Biemiller, J. (2021). The mechanics of creep, slow slip events and earthquakes in mixed brittle-ductile fault zones. *Journal of Geophysical Research: Solid Earth*, e2020JB020325.

Lay, T., Kanamori, H., Ammon, C. J., Koper, K. D., Hutko, A. R., Ye, L., … Rushing, T. M. (2012). Depth-varying rupture properties of subduction zone megathrust faults. *Journal of Geophysical Research: Solid Earth*, *117*(B4).

Leeman, J., Saffer, D., Scuderi, M., & Marone, C. (2016). Laboratory observations of slow earthquakes and the spectrum of tectonic fault slip modes. *Nature communications*, *7*(1), 1–6.

Li, J., Shillington, D. J., Bécel, A., Nedimović, M. R., Webb, S. C., Saffer, D. M., … Kuehn, H. (2015). Downdip variations in seismic reflection character: Implications for fault structure and seismogenic behavior in the alaska subduction zone. *Journal of Geophysical Research: Solid Earth*, *120*(11), 7883–7904.

Liu, Y., & Rice, J. (2005). Aseismic slip transients emerge spontaneously in three-dimensional rate and state modeling of subduction earthquake sequences. *Journal of Geophysical Research*, *110*(B8).

Liu, Y., & Rubin, A. M. (2010). Role of fault gouge dilatancy on aseismic deformation transients. *Journal of Geophysical Research*, *115*(B10).

Marone, C. (1998). Laboratory-derived friction laws and their application to seismic faulting. *Annual Review of Earth and Planetary Sciences*, *26*(1), 643–696.

Marone, C., Vidale, J. E., & Ellsworth, W. L. (1995). Fault healing inferred from time dependent variations in source properties of repeating earthquakes. *Geophysical Research Letters*, *22*(22), 3095–3098.

Marroni, M., Pandolfi, L., Principi, G., Malasoma, A., & Meneghini, F. (2009). Deformation history of the eclogite-and jadeitite-bearing mélange from north motagua fault zone, guatemala: insights in the processes of a fossil subduction channel. *Geological Journal*, *44*(2), 167–190.

McLaskey, G. C., Thomas, A. M., Glaser, S. D., & Nadeau, R. M. (2012). Fault healing promotes high-frequency earthquakes in laboratory experiments and on natural faults. *Nature*, *491*(7422), 101–104.

Michel, S., Gualandi, A., & Avouac, J.-P. (2019). Similar scaling laws for earthquakes and cascadia slow-slip events. *Nature*, *574*(7779), 522–526.

Nakata, R., Ando, R., Hori, T., & Ide, S. (2011). Generation mechanism of slow earthquakes: Numerical analysis based on a dynamic model with brittle-ductile mixed fault heterogeneity. *Journal of Geophysical Research*, *116*(B8).

Nedimović, M. R., Hyndman, R. D., Ramachandran, K., & Spence, G. D. (2003). Reflection signature of seismic and aseismic slip on the northern cascadia subduction interface. *Nature*, *424*(6947), 416–420.

Obara, K. (2002, May). Nonvolcanic deep tremor associated with subduction in southwest japan. *Science*, *296*(5573), 1679–1681.

Obara, K., Matsuzawa, T., Tanaka, S., & Maeda, T. (2012). Depth-dependent mode of tremor migration beneath kii peninsula, nankai subduction zone. *Geophysical research letters*, *39*(10).

Obara, K., & Sekine, S. (2009). Characteristic activity and migration of episodic tremor and slow-slip events in central japan. *Earth, Planets and Space*, *61*(7), 853–862.

Peacock, S. M. (2009). Thermal and metamorphic environment of subduction zone episodic tremor and slip. *Journal of Geophysical Research*, *114*.

Peacock, S. M., Christensen, N. I., Bostock, M. G., & Audet, P. (2011). High pore pressures and porosity at 35 km depth in the cascadia subduction zone. *Geology*, *39*(5), 471–474.

Peng, Y., Rubin, A. M., Bostock, M. G., & Armbruster, J. G. (2015). High-resolution imaging of rapid tremor migrations beneath southern vancouver island using cross-station cross correlations. *Journal of Geophysical Research: Solid Earth*, *120*(6), 4317–4332.

Peng, Z., & Gomberg, J. (2010). An integrated perspective of the continuum between earthquakes and slow-slip phenomena. *Nature Geoscience*, *3*(9), 599–607.

Petrini, C., Gerya, T., Yarushina, V., van Dinther, Y., Connolly, J., & Madonna, C. (2020). Seismo-hydro-mechanical modelling of the seismic cycle: methodology and implications for subduction zone seismicity. *Tectonophysics*, *791*, 228504.

Phillips, N. J., Motohashi, G., Ujiie, K., & Rowe, C. D. (2020). Evidence of localized failure along altered basaltic blocks in tectonic mélange at the updip limit of the seismogenic zone: Implications for the shallow slow earthquake source. *Geochemistry, Geophysics, Geosystems*, *21*(7), e2019GC008839.

Platt, J. P., Xia, H., & Schmidt, W. L. (2018). Rheology and stress in subduction zones around the aseismic/seismic transition. *Progress in Earth and Planetary Science*, *5*(1), 1–12.

Preuss, S., Herrendörfer, R., Gerya, T., Ampuero, J.-P., & van Dinther, Y. (2019). Seismic and aseismic fault growth lead to different fault orientations. *Journal of Geophysical Research: Solid Earth*, *124*(8), 8867–8889.

Rad, G. F., Droop, G., Amini, S., & Moazzen, M. (2005). Eclogites and blueschists of the sistan suture zone, eastern iran: a comparison of P–T histories from a subduction mélange. *Lithos*, *84*(1-2), 1–24.

Reber, J. E., Lavier, L. L., & Hayman, N. W. (2015). Experimental demonstration of a semi-brittle origin for crustal strain transients. *Nature Geoscience*, *8*(9), 712–715.

Rice, J. R., Lapusta, N., & Ranjith, K. (2001). Rate and state dependent friction and the stability of sliding between elastically deformable solids. *Journal of the Mechanics and Physics of Solids*, *49*(9), 1865–1898.

Rogers, G., & Dragert, H. (2003, June). Episodic tremor and slip on the cascadia subduction zone: the chatter of silent slip. *Science*, *300*(5627), 1942–1943.

Rousset, B., Campillo, M., Lasserre, C., Frank, W. B., Cotte, N., Walpersdorf, A., ... Kostoglodov, V. (2017). A geodetic matched filter search for slow slip with application to the mexico subduction zone. *Journal of Geophysical Research: Solid Earth*, *122*(12), 10–498.

Rousset, B., Fu, Y., Bartlow, N., & Bürgmann, R. (2019). Weeks-Long and Years-Long slow slip and tectonic tremor episodes on the south central alaska megathrust. *Journal of Geophysical Research: Solid Earth*, *124*(12), 13392–13403.

Rubin, A. M. (2008). Episodic slow slip events and rate-and-state friction. *Journal of Geophysical Research*, *113*(B11).

Rubin, A. M., & Ampuero, J.-P. (2005). Earthquake nucleation on (aging) rate and state faults. *Journal of Geophysical Research: Solid Earth*, *110*(B11).

Rubin, A. M., & Armbruster, J. G. (2013). Imaging slow slip fronts in cascadia with high precision cross-station tremor locations. *Geochemistry, Geophysics, Geosystems*, *14*(12), 5371–5392.

Ruina, A. (1983). Slip instability and state variable friction laws. *Journal of Geophysical Research: Solid Earth*, *88*(B12), 10359–10370.

Scarsi, M., Malatesta, C., & Fornasaro, S. (2018). Lawsonite-bearing eclogite from a tectonic mélange in the ligurian alps: New constraints for the subduction plate-interface evolution. *Geological Magazine*, *155*(2), 280–297.

Schmidt, D. A., & Gao, H. (2010). Source parameters and time-dependent slip distributions of slow slip events on the cascadia subduction zone from 1998 to 2008. *Journal of Geophysical Research*, *115*.

Segall, P., & Bradley, A. M. (2012). The role of thermal pressurization and dilatancy in controlling the rate of fault slip. *Journal of Applied Mechanics*, *79*(3).

Segall, P., Rubin, A. M., Bradley, A. M., & Rice, J. R. (2010). Dilatant strengthening as a mechanism for slow slip events. *Journal of Geophysical Research*, *115*(B12).

Shelly, D. R. (2017). A 15 year catalog of more than 1 million low-frequency earthquakes: Tracking tremor and slip along the deep san andreas fault. *Journal of Geophysical Research: Solid Earth*, *122*(5), 3739–3753.

Shelly, D. R., Beroza, G. C., & Ide, S. (2007). Non-volcanic tremor and low-frequency earthquake swarms. *Nature*, *446*(7133), 305–307.

Shelly, D. R., Beroza, G. C., Ide, S., & Nakamula, S. (2006, July). Low-frequency earthquakes in shikoku, japan, and their relationship to episodic tremor and slip. *Nature*, *442*(7099), 188–191.

Shibazaki, B. (2003). On the physical mechanism of silent slip events along the deeper part of the seismogenic zone. *Geophysical Research Letters*, *30*(9).

Sibson, R. (1992). Implications of fault-valve behaviour for rupture nucleation and recurrence. *Tectonophysics*, *211*(1-4), 283–293.

Skarbek, R. M., Rempel, A. W., & Schmidt, D. A. (2012). Geologic heterogeneity can produce aseismic slip transients. *Geophysical Research Letters*, *39*(21).

Stöckhert, B. (2002). Stress and deformation in subduction zones: insight from the record of exhumed metamorphic rocks. *Geological Society, London, Special Publications*, *200*(1), 255–274.

Suzuki, T., & Yamashita, T. (2009). Dynamic modeling of slow earthquakes based on thermoporoelastic effects and inelastic generation of pores. *Journal of Geophysical Research*, *114*.

Taetz, S., John, T., Bröcker, M., Spandler, C., & Stracke, A. (2018). Fast intraslab fluid-flow events linked to pulses of high pore fluid pressure at the subducted plate interface. *Earth and Planetary Science Letters*, *482*, 33–43.

Takagi, R., Obara, K., & Maeda, T. (2016). Slow slip event within a gap between tremor and locked zones in the nankai subduction zone. *Geophysical Research Letters*, *43*(3), 1066–1074.

Tarling, M. S., Smith, S. A., & Scott, J. M. (2019). Fluid overpressure from chemical reactions in serpentinite within the source region of deep episodic tremor. *Nature Geoscience*, *12*(12), 1034–1042.

Tewksbury-Christle, C., Behr, W., & Helper, M. (2021). Tracking deep sediment underplating in a fossil subduction margin: implications for interface rheology and mass and volatile recycling. *Geophysics, Geochemistry, Geosystems*, *in press*. doi: 10.1029/2020GC009463

Thomas, A. M., Nadeau, R. M., & Bürgmann, R. (2009). Tremor-tide correlations and near-lithostatic pore pressure on the deep san andreas fault. *Nature*, *462*(7276), 1048–1051.

Ujiie, K., Saishu, H., Fagereng, Å., Nishiyama, N., Otsubo, M., Masuyama, H., & Kagi, H. (2018). An explanation of episodic tremor and slow slip constrained by crack-seal veins and viscous shear in subduction mélange. *Geophysical Research Letters*, *45*(11), 5371–5379.

Ukar, E., & Cloos, M. (2019). Cataclastic deformation and metasomatism in the subduction zone of mafic blocks-in-mélange, san simeon, california. *Lithos*, *346*, 105116.

van Dinther, Y., Gerya, T., Dalguer, L., Mai, P. M., Morra, G., & Giardini, D. (2013). The seismic cycle at subduction thrusts: Insights from seismo-thermo-mechanical models. *Journal of Geophysical Research: Solid Earth*, *118*(12), 6183–6202.

Wallace, L. M., & Eberhart-Phillips, D. (2013). Newly observed, deep slow slip events at the central hikurangi margin, new zealand: Implications for downdip variability of slow slip and tremor, and relationship to seismic structure. *Geophysical Research Letters*, *40*(20), 5393–5398.

Warren-Smith, E., Fry, B., Wallace, L., Chon, E., Henrys, S., Sheehan, A., … Lebedev, S. (2019). Episodic stress and fluid pressure cycling in subducting oceanic crust during slow slip. *Nature Geoscience*, *12*(6), 475–481.

Wassmann, S., & Stoeckhert, B. (2013). Rheology of the plate interface—dissolution precipitation creep in high pressure metamorphic rocks. *Tectonophysics*, *608*, 1–29.

Wech, A. G., & Bartlow, N. M. (2014). Slip rate and tremor genesis in Cascadia. *Geophysical Research Letters*, *41*(2), 392–398.

Wech, A. G., Boese, C. M., Stern, T. A., & Townend, J. (2012). Tectonic tremor and deep slow slip on the alpine fault. *Geophysical Research Letters*, *39*(10).

Xia, H., & Platt, J. P. (2017). Structural and rheological evolution of the laramide subduction channel in southern california. *Solid Earth*, *8*(2), 379–403.

Yamato, P., Duretz, T., & Angiboust, S. (2019). Brittle/ductile deformation of eclogites: insights from numerical models. *Geochemistry, Geophysics, Geosystems*, *20*(7), 3116–3133.